The Journal of Experimental Biology 211, 3378-3391
Published by The Company of Biologists 2008
doi:10.1242/jeb.023564

Biomechanics of a convergently derived prey-processing mechanism in fishes: evidence from comparative tongue bite apparatus morphology and raking kinematics

Nicolai Konow* and Christopher P. J. Sanford
Department of Biology, 114 Hofstra University, Hempstead, NY 11549, USA
*Author for correspondence (e-mail: nkonow@jhmi)

Accepted 25 August 2008

SUMMARY

A tongue-bite apparatus (TBA) governs raking behaviors in two major and unrelated teleost lineages, the osteoglossomorph and salmoniform fishes. We present data on comparative morphology and kinematics from two representative species, the rainbow trout (*Oncorhynchus mykiss*) and the Australian arowana (*Scleropages jardinii*), which suggest that both the TBA and raking are convergently derived in these lineages. Similar TBA morphologies were present, except for differences in TBA dentition and shape of the novel cleithrobranchial ligament (CBL), which is arc-shaped in *O. mykiss* and straight in *S. jardinii*. Eight kinematic variables were used to quantify motion magnitude and maximum-timing in the kinematic input mechanisms of the TBA. Five variables differed inter-specifically (pectoral girdle retraction magnitude and timing, cranial and hyoid elevation and gape-distance timing), yet an incomplete taxon separation across multivariate kinematic space demonstrated an overall similarity in raking behavior. An outgroup analysis using bowfin (*Amia calva*) and pickerel (*Esox americanus*) to compare kinematics of raking with chewing and prey-capture provided robust quantitative evidence of raking being a convergently derived behavior. Support was also found for the notion that raking more likely evolved from the strike, a functionally distinct behavior, than from chewing, an alternative prey-processing behavior. Based on raking kinematic and muscle-activity data, we propose biomechanical models of the three input mechanisms that govern kinematics of the basihyal output mechanism during the raking power stroke: (1) cranial elevation protracts the upper TBA jaw from the lower (basihyal) TBA jaw; (2) basihyal retraction is caused directly by contraction of the sternohyoideus (SH); (3) hypaxial shortening, relayed *via* the pectoral girdle and SH–CBL complex, is an indirect basihyal retraction mechanism modeled as a four-bar linkage. These models will aid future analyses mapping structural and functional traits to the evolution of behaviors.

Supplementary material available online at http://jeb.biologists.org/cgi/content/full/211/21/3378/DC1

Key words: biomechanics, aquatic, feeding, behavior, fish, prey capture.

INTRODUCTION

The functional morphology of prey-capture has been studied much more extensively than the diverse range of prey-processing behaviors that exist among aquatic-feeding vertebrates (Ferry-Graham and Lauder, 2001). One notable exception, pharyngeal mastication, is governed by a functionally unique pharyngeal jaw apparatus (PJA), which decouples the primary mandibular jaw apparatus from prey-processing tasks (Sibbing, 1982; Grubich, 2003; Wainwright, 2005). The PJA is thus mechanically and functionally distinct from the mandibular jaws (Wainwright and Turingan, 1993; Wainwright, 2005). By contrast, most other prey-processing behaviors, including chewing (Gillis and Lauder, 1995; Lauder, 1980; Lauder, 1981; Lauder, 1982; Sanford and Lauder, 1990), winnowing (Drucker and Jensen, 1991) and blowing (Turingan et al., 1995; Turingan and Wainwright, 1993), are closely coupled with the mandibular jaws *via* musculoskeletal links. The hyolingual 'tongue-bite apparatus' (TBA) is a third set of jaws situated between the oral and pharyngeal jaws in two major teleost lineages, the osteoglossomorph and salmonid fishes (Lauder and Liem, 1983; Sanford and Lauder, 1989). Given the distant relationship between these two groups (Ishiguro et al., 2003) (Fig. 1), the evolution of a TBA connected to the pre-existing jaw apparatus by shared morphology may provide an interesting model system of how coupled musculoskeletal form and function evolve convergently to govern a derived behavioral theme (Lauder and Reilly, 1994).

Several diagnostic characters are present in the TBAs of both raking lineages [and also in some argentinoids and osmeroids (Rosen, 1974; Lauder and Liem, 1983)] but absent in outgroup taxa (Fig. 1). These include (1) tooth plates or dentition on the basihyal, which is heavily ossified; (2) directly opposing tooth plates or individual teeth on the vomer, parasphenoid and, more laterally, the dermopalatine and pterygoid mouth-roofing bones [together forming the tongue-bite (see Sanford and Lauder, 1989; Hilton, 2001)] and (3) a cleithrobranchial ligament (CBL) (Ridewood, 1904; Ridewood, 1905; Nelson, 1968; Greenwood, 1971; Greenwood, 1973; Kershaw, 1976; Taverne, 1979; Sanford and Lauder, 1989; Sanford and Lauder, 1990; Sanford, 2001b; Hilton, 2001; Hilton, 2003). While it has been suggested that the TBA is a convergently derived jaw apparatus (Sanford and Lauder, 1989), TBA morphology has never been compared between members of the two raking lineages, which would indicate to what extent lineage-typical TBAs are structurally equivalent. Moreover, detailed TBA morphology has only been examined in osteoglossomorphs, where considerable structural disparity, particularly in dentition morphology and distribution, is found (Ridewood, 1904; Ridewood, 1905; Greenwood, 1973; Taverne, 1979; Hilton, 2003). By contrast, a superficially conservative cranial anatomy among salmonids may reflect a restricted TBA morphological disparity (Lauder and Liem, 1980; Sanford, 2000; Sanford, 2001b).

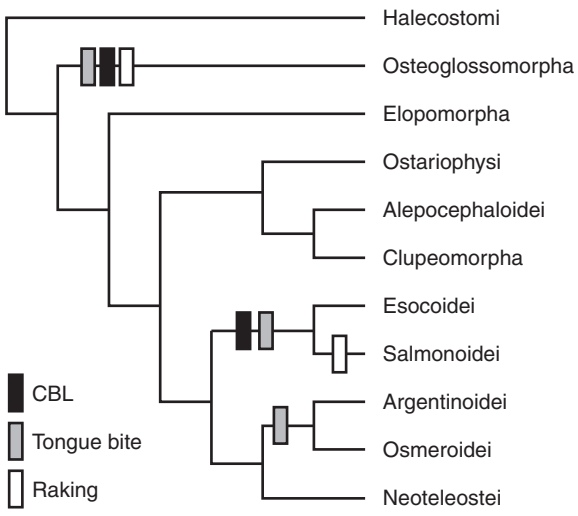

Fig. 1. Phylogeny for the 'Ancient fishes' following Ishiguro et al. (Ishiguro et al., 2003) with trait-mapping to clades (maximum parsimony; Mesquite v. 2.01; http://mesquiteproject.org) identifying the presence of a cleithrobranchial ligament (CBL), a tongue bite (see text) and raking behavior. Morphology data (Sanford and Lauder, 1989; Sanford, 2001b); for TBA (Nelson, 1968; Greenwood, 1971; Rosen, 1974; Taverne, 1977; Taverne, 1978; Lauder and Liem, 1983; Hilton, 2001); behavioral data (Kershaw, 1976; Sanford and Lauder, 1989; Sanford and Lauder, 1990; Sanford, 2001a; Sanford, 2001b).

A novel raking prey-processing behavior is directly associated with the TBA, involving characteristic kinematics that may be ubiquitous but so far only quantified in a phylogenetically diverse osteoglossomorph sample. Osteoglossomorph raking kinematics divides into two categories. The first category is primarily driven by pectoral girdle excursion and augmented by cranial elevation, exemplified by *Chitala*, a notopterid knifefish (Sanford and Lauder, 1989; Sanford and Lauder, 1990; Frost and Sanford, 1999). The CBL extends medially through the sternohyoideus (SH) muscle from the pectoral girdle to the hyoid bar and, in *Chitala* and other raking taxa, this ligament may structurally duplicate the ancestral muscular connection. As such, the CBL may provide a more direct link for translation of hypaxialis muscle strain into basihyal retraction during raking (Sanford and Lauder, 1989; Hilton, 2003). By contrast, the second category of raking is primarily driven by cranial elevation and augmented by pectoral girdle retraction. This category is found in *Osteoglossum* (silver arowana), *Pantodon* (African butterflyfish) and *Xenomystus* (African knifefish) (Sanford and Lauder, 1990; Sanford, 2001a); a cranial elevation driven pattern is also present in *Salvelinus fontinalis* (brook trout), the only taxon for which there is quantitative data on salmonid raking kinematics (Lauder and Liem, 1980; Sanford, 2001b).

Differentiation of raking kinematics from alternative prey-processing (chewing) and functionally distinct behaviors (e.g. prey capture) within each lineage has been thoroughly quantified (Sanford and Lauder, 1989; Sanford and Lauder, 1990; Frost and Sanford, 1999; Sanford, 2001a; Konow et al., 2008). However, it remains to be quantitatively demonstrated if raking is convergently derived in the TBA-bearing lineages. The absence of similar kinematic movements (Lauder, 1979; Lauder, 1982; Liem, 1990; Sanford and Lauder, 1989) in the feeding behavioral repertoires of outgroup teleosts, including *Amia* (Lauder, 1980) and *Esox* (Rand and Lauder, 1981), suggests that raking is a derived behavior (Fig. 1; Table 1A). Raking involves extensive cranial elevation but also sustained oral jaw occlusion past the preparatory phase (Table 1B). Raking can also be divided into a distinct preparatory, power-stroke and recovery phase, suggesting that raking resembles a (hypothetical) 'closed-mouth strike' (Sanford, 2001a; Sanford, 2001b). However, since the oral jaws are tightly occluded during the different phases of raking (Frost and Sanford, 1999; Sanford, 2001b), concomitant cranial elevation and pectoral girdle retraction may result in hyoid kinematics that differ distinctly from the typical hyoid depression generated during strikes (Anker, 1974; Muller, 1987; Sanford and Wainwright, 2002). The resulting TBA kinesis has been suggested to involve more antero-posteriorly directed basihyal motion (Sanford and Lauder, 1989; Hilton, 2003), and ejected prey debris indicates that considerable prey reduction results from the raking power-stroke kinesis. Moreover, opercular flaring, which is commonly observed during raking, may be caused by the hyoid bars passively abducting the suspensorium (Muller, 1987; Muller, 1989; De Visser and Barel, 1996).

Despite the interesting implications of novel raking kinematics, a lack of muscle-activity data has, until recently, prevented determination of whether raking is driven by a convergently derived muscle activity pattern (MAP) (Sanford and Lauder, 1989). This is a logical hypothesis, given the clear functional shifts from prey capture and alternative prey-processing behaviors outlined above (Alfaro and Herrel, 2001; Wainwright, 2005). Raking MAP data from the rainbow trout (*Oncorhynchus mykiss*) and the osteoglossomorph arowana (*Scleropages jardinii*) now reveal that a convergently derived MAP is indeed responsible for basihyal protraction and mandibular jaw occlusion during the raking preparatory phase (Konow and Sanford, 2008). However, since subtle interspecific differences were present in the subsequent raking power-stroke MAPs, exploration of the diversity in TBA morphology and raking kinematics in these taxa is important. The ability to predict changes in kinematics based on morphological differences is a key goal in functional biology, and thus the TBA provides a new system for analyses of links between organizational levels (Sanford and Lauder, 1989; Sanford and Lauder, 1990; Frost and Sanford, 1999; Sanford, 2001a; Sanford, 2001b).

Biomechanical models are valuable tools in quantitative analyses of musculoskeletal mechanisms during teleost prey-capture (Anker, 1974; Muller, 1987; Westneat, 1994; Westneat, 1995; Westneat, 2003; Westneat, 2004). Conversely, prey-processing mechanisms have generally been examined indirectly or purely descriptively (see also Sibbing, 1982; Drucker and Jensen, 1991; Hernandez and Motta, 1997), with the exception of sciaenid pharyngeal jaw mastication, which is a decoupled feeding mechanism (Grubich, 2003; Grubich, 2005; Grubich and Westneat, 2006). Existing prey-capture models suggest that the specific contributions of distinct input mechanisms (e.g. cranial elevation) are important factors in shaping the mechanistic output (i.e. basihyal motion-pattern). Thus, biomechanical models based on TBA morphology, raking kinematics and muscle activity in a novel musculoskeletal system (the TBA) can help identify how the individual component mechanisms interact to shape the resulting behavior.

Our main aims are therefore to compare TBA morphology and raking kinematics in *O. mykiss* and *S. jardinii*. These taxa have relatively similar raking muscle activity patterns (Konow and Sanford, 2008) and, given evidence from their close sister taxa, they may also use relatively similar raking kinematics (see above) (see also Sanford and Lauder, 1990; Sanford, 2001b). Each taxon is a phylogenetic intermediate in its respective lineage – an advantageous taxon pairing that may reveal subtle differences in input kinematics,

Table 1. Similarities and differences in (A) kinematics and (B) behavioural phases between raking and alternative feeding behaviours among teleost fishes

A

Mechanisms	Raking	Strike	Chewing	Taxa	Study
Neurocranium	Elevation +++	Elevation +++	Elevation +	*Micropterus, Chitala, Osteoglossum, Salvelinus*	Carroll, 2004; Thys, 1997; Sanford and Lauder, 1989; Frost and Sanford, 1999; Sanford, 2001b
Pectoral girdle	Retraction +++	Retraction +++	Retraction +	*Notopterus, Osteoglossum*	Sanford and Lauder, 1989; Sanford and Lauder, 1990
Oral jaws	Occlusion +	Expansion +++	Expansion to occlusion +++	*Chitala, Osteoglossum, Salvelinus*	Motta, 1984; Sanford and Lauder, 1989; Sanford and Lauder, 1990; Sanford, 2001a; Sanford, 2001b
Hyoid bar	Protraction to retraction	Depression	Depression	*Salvelinus, Chitala, Osteoglossum, Micropterus*	Muller, 1987; Sanford, 2001b; Sanford and Lauder, 1989; Sanford and Lauder, 1990; Sanford, 2001a; Sanford and Wainwright, 2002
Suspensorium	Flaring	Flaring	Occlusion	*Lepisosteus, Polypterus, Amia, Chitala*	Lauder, 1980; Muller, 1987; Muller, 1989; Sanford, 2001a

B

Oral and buccal cavities	Raking	Strike	Chewing	Reference
Preparatory phase	Compressive	Compressive	Expansive	Lauder, 1980; Lauder,1981; Muller, 1987; Sanford and Lauder, 1989; Sanford and Lauder, 1990; Gillis and Lauder, 1995; Frost and Sanford, 1999; Sanford, 2001a; Sanford, 2001b; Sanford and Wainwright, 2002
Power stroke phase	Compressive	Expansive to compressive	Compressive	
Recovery phase	Expansive	Expansive	Expansive	

See Sanford and Lauder (Sanford and Lauder, 1989), and Hilton (Hilton, 2001) for treatments of tongue-bite apparatus traits in raking teleosts.
Underlined reference indicates source for underlined trait.
+, modest; ++, considerable; +++, extensive kinematic excursion.

which potentially could be obscured by secondary modifications of raking kinematics and muscle activity in alternative pairs (Konow et al., 2008). Specifically, we examine TBA morphology of these representatives to test the hypothesis that the TBAs in members of the two raking lineages are morphologically equivalent or, alternatively, that fundamental differences may exist in TBA morphology. We compare raking input kinematics of the mandible, hyoid, neurocranium and pectoral girdle to quantitatively test whether raking kinematics exhibit convergent or divergent trends with the underlying muscle-activity patterns in these taxa (Konow and Sanford, 2008). Comparison of raking input kinematics with those of alternative chewing prey-processing and functionally distinct strike behaviors in both ingroup and outgroup taxa (*Amia* and *Esox*) test whether raking kinematics is convergently derived in the TBA-bearing lineages. Finally, we derive TBA biomechanical models from comparative morphology, kinematics and muscle activity evidence to obtain a theoretical framework for future quantitative studies aiming to categorize a larger taxon sample into functional groups, determined by the relative contribution of input mechanisms.

MATERIALS AND METHODS

Specimen and husbandry

Four size-matched specimens of rainbow trout, *Oncorhynchus mykiss* (Walbaum 1792), with head lengths (HL) ranging from 3.7 to 4.1 cm (mean ± s.e.m.=4.0±0.1 cm) were obtained from the Cold Spring Harbor Fish Hatchery, NY, USA. Four equal-sized Australian arowana, *Scleropages jardinii* (Saville-Kent 1892), with HL ranging from 3.95 to 4.55 cm (mean ± s.e.m.=4.26±0.25 cm) were purchased from retail aquarium stores. Strike and chew data for the outgroup analysis of feeding kinematics (see below) were later obtained from three individuals of each species: *O. mykiss* (HL range 3.6–7.4 cm); *S. jardinii* (HL range 4.1–6.7 cm); *Amia calva* (HL range 5.4–5.5 cm) and *Esox americanus* (HL range 4.7–7.4 cm). There were no significant differences between HL ranges of these species (ANOVA; P=0.21). Specimens were thus adequately size-matched to avoid potential kinematic scaling effects (Richard and Wainwright, 1995). Specimens were housed individually at 15°C for *O. mykiss* and 25°C for the three other taxa in the Hofstra University animal care facility, in accordance with applicable ethics and animal-care approvals. During acclimation, daily provisioning included a mix of naturally encountered prey types, i.e. Canadian nightcrawlers (*Lumbricus*), crickets (*Gryllus*), goldfish (*Carassius*) and minnows (*Pimephales*), to avoid possible habituation effects on feeding behavior. Experiments started when specimens were feeding aggressively under floodlight illumination and otherwise appeared well acclimated.

Morphological examinations

Additional specimens (N=3 per species) were euthanized in an alcoholic Eugenol (clove oil) overdose, used for manipulation studies, then fixed in 10% isotonic-buffered formalin, skinned and eviscerated, and clear-stained for bone and cartilage (Dingerkus and Uhler, 1977). Cleared and stained specimens were then dissected and step-photographed under an Olympus SZX12 dissecting microscope with a digital camera. TBA diagrams were traced from the resulting series of still images using Corel Draw v. 12.

Video recording

Specimens were video recorded whilst feeding in their home aquaria, with a background Plexiglas grid marked in 1 cm squares for scaling purposes, located ~120 mm from the front window to minimize parallax resulting from animal movement perpendicular to the lens axis. Independent scale verification showed the measuring

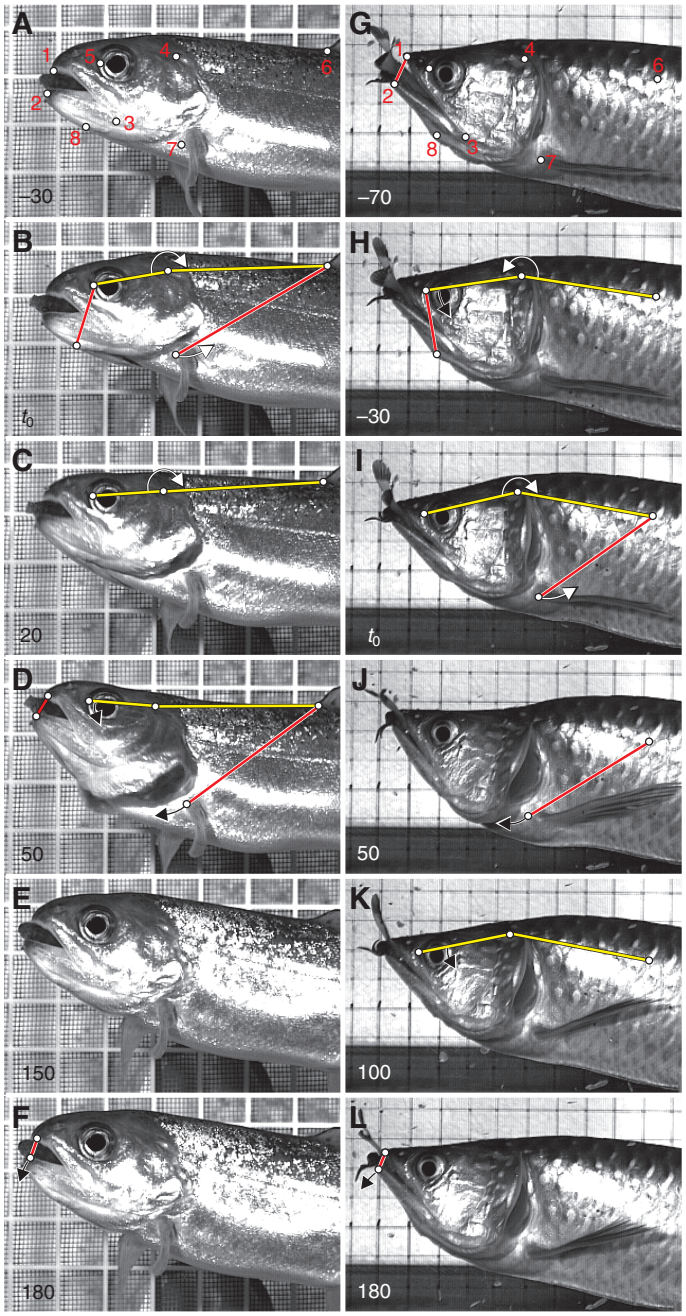

Fig. 2. High-speed video image series from representative movie sequences of raking in *O. mykiss* and *S. jardinii*. The typical stages of a rake seen in each taxon are illustrated with their mean timing relative to t_0 indicated (in ms) at the bottom left corner of each frame. The primary kinematic variables were calculated from motion analysis of the eight topographical points shown in A and G (see text for details). Kinematic displacement, indicated with yellow lines for angular and red lines for linear displacement, in each frame becomes apparent in the following frame. White arrows indicate displacement and grey arrows indicate subsequent variable recovery. *O. mykiss*: (A) preparatory phase (gape occlusion and lower jaw elevation); (B) t_0 (onset of cranial elevation, followed by pectoral girdle retraction); (C) completion of cranial elevation; (D) completion of power stroke, followed by recovery phase (cranial depression and pectoral girdle protraction); (E) common pause in kinematics; (F) gape expansion and lower jaw angle recovery. *S. jardinii*: (G) preparatory phase (gape occlusion and lower jaw elevation); (H) preparatory cranial depression; (I) t_0 (onset of cranial elevation and hyoid elevation); (J) pectoral girdle retraction, to completion of power stroke; (K) recovery phase initiated by cranial depression and pectoral girdle protraction; (L) gape expansion.

error resulting from a displacement of the fish from the background grid to the front of the tank to be <0.5 pixels. Two 600 W floodlights provided illumination during video recording. Experimental prey consisted of goldfish with a total length of 3–4 cm, equaling predator mouth width. Goldfish prey were released live into the feeding arena containing the predator, which typically caught the prey in a voracious strike, and proceeded with prey-processing over a period ranging from 1 to 300 s before the prey was swallowed. Two days of food deprivation elapsed between each filming event to ensure voracious predator behavior. Despite the voracious nature of these predators, each experiment only consisted of two feedings, since satiation affects predator performance (Sass and Motta, 2002; Robinson and Motta, 2002). Therefore, feeding events were filmed over ⩽20 days to secure enough digitizable sequences. Video was recorded using an NAC HSV-500 camera (Simi Valley, CA, USA), in black and white for maximal contrast, onto super VHS tapes at 250 frames s^{-1}. Additional sequences were filmed using a Photron Fastcam-X 1280 PCI camera (San Diego, CA, USA). The camera focused on the anterior half of the fish (Fig. 2) so that feeding head movements could be clearly identified.

Kinematics

Video files were batch-grabbed to PC hard drive as uncompressed (raw) AVI files, which were then scrutinized for aberrant predator behavior, and five representative rake sequences of each individual were selected and cropped for analysis in Virtual Dub (v. 1.6; http://virtualdub.org/). In order to obtain comparable data on raking kinematics from both taxa, we only analysed video sequences containing the preparatory, power-stroke and recovery phases of the rake (Fig. 2). The raking power-stroke onset, or 'time-zero' (t_0), was designated as one frame prior to the rapid increase in cranial elevation, which could be easily identified among all feeding sequences. Video sequences selected for analysis were digitized at 8 ms intervals (every second field) for 80 ms prior to, and 200 ms after, t_0 (36 frames per sequence). For all four individuals of each taxon, five raking sequences were analyzed. Previous work has shown that 125 Hz (8 ms) is an effective sample frequency for video analysis of these behaviors (Frost and Sanford, 1999).

The selected and cropped video files were imported to TEMA v. 2.2 (Image Systems AB, Linköping, Sweden) for data-extraction using landmark motion-tracking at frame-by-frame (8 ms) increments. In order to quantify cranial kinesis during raking (Fig. 1), the following eight landmarks were tracked: (1) the anterior upper jaw tip, (2) the anterior lower jaw tip, (3) the lower jaw (quadrate–articular) joint, (4) the dorsal and anterior-most opercular margin (morphological examinations determined that this landmark is a reliable surface proxy for the cranio-vertebral and cranio-pectoral girdle articulations), (5) the anterior-ventral corner of the orbit, (6) the body at the anterior insertion of the first dorsal fin, or alternatively an identifiable mark in the same general area, to provide a post-cranial point in the fish's frame of reference, (7) the anterior-most point of pectoral fin insertion, (8) the antero-ventral tip of the hyoid.

Resultant 2-D coordinates (x, y) from motion analysis of each landmark were used to calculate the following four kinematic variables (Fig. 4), describing linear and angular displacements in the head during raking (in the fish's frame of reference): (i) vertical gape distance, measured in cm from point 1 to 2; (ii) hyoid distance, measured in cm as the vertical distance 5–8; we chose this measure, as a proxy for the basihyal dorsoventral movement relative to the ventral surface of the prey, and it may reflect compressive forces from the TBA onto the prey; this measure does

Table 2. Summary of kinematic variables in (A) ingroup and (B) outgroup taxa studied

A. ingroup taxa

	Oncorhynchus mykiss			*Scleropages jardinii*		
	Rake	Chew	Strike	Rake	Chew	Strike
Magnitude						
Cranial elevation (deg.)	22.41±1.62	7.79±1.38	14.50±3.10	13.05±1.45	6.01±2.52	11.26±4.57
Gape distance (mm)	1.57±0.25	14.70±0.72	19.13±0.86	0.81±0.17	5.56±1.01	10.23±1.74
Pectoral girdle retraction (mm)	7.51±0.34	2.53±0.50	3.47±0.80	4.07±0.51	1.86±0.64	1.57±0.91
Hyoid distance (mm)	1.30±0.20	12.19±0.50	14.98±1.12	1.28±0.21	6.48±0.93	5.34±1.18
Timing (from t_0)						
Max. cranial elevation (ms)	44.30±0.71	46.45±1.18	67.03±2.74	50.24±0.73	47.96±1.59	40.15±1.77
Max. gape distance (ms)	49.50±1.19	49.26±1.39	63.05±2.88	66.38±1.13	36.40±2.15	29.90±2.06
Max. pectoral girdle retraction (ms)	44.30±0.71	45.60±1.33	81.00±3.25	38.19±1.04	31.20±1.21	36.00±0.00
Hyoid distance (ms)	35.00±0.79	50.75±1.35	59.03±2.51	53.64±1.20	38.38±1.84	38.05±2.67

B. outgroup taxa

	Amia calva		*Esox americanus*	
	Chew	Strike	Chew	Strike
Magnitude				
Cranial elevation (deg.)	3.89±1.62	11.87±3.65	3.21±2.65	22.29±4.20
Gape distance (mm)	28.57±2.49	22.86±1.22	7.07±1.11	26.59±1.58
Pectoral girdle retraction (mm)	19.51±1.71	4.60±0.97	1.38±0.41	5.73±1.14
Hyoid distance (mm)	36.82±2.22	21.44±1.36	4.69±0.83	27.90±1.60
Timing (from t_0)				
Cranial elevation (ms)	64.82±2.17	70.22±2.69	125.87±3.90	73.42±2.65
Gape distance (ms)	82.90±2.63	63.47±2.92	102.22±3.42	63.88±2.97
Pectoral girdle retraction (ms)	88.80±2.51	78.20±3.14	90.67±4.05	75.40±3.03
Hyoid distance (ms)	89.18±2.66	64.73±2.77	119.90±3.68	70.44±3.02

Values are means ± s.e.m.

not, however, reflect the hypothesized anteroposterior basihyal raking motion, as such movements of the hyoid are poorly quantifiable *via* external motion analyses (Sanford and Wainwright, 2002) and are a topic for forthcoming analyses (N.K. and C.P.J.S., unpublished data); (iii) cranial elevation, measured as the angle 5,4,6, with 4 as vertex; this angle reflects the anterior-dorsal rotation of the TBA upper jaw during raking; and (iv) pectoral girdle displacement after t_0; pectoral girdle displacement in the fish's frame of reference was calculated in cm using the absolute (x,y coordinate) position at time t_1–t_0 subtracted from the reference point on the body (6). The pectoral girdle is biomechanically linked to the lower TBA by both the SH muscle and a derived cleithrobranchial ligament (Fig. 3). Therefore, pectoral girdle retraction causes a posterior-directed movement of the ventral TBA jaw. Theoretically, based on existing analyses of TBA functional morphology (Rosen, 1974; Lauder and Liem, 1983; Sanford and Lauder, 1989; Sanford and Lauder, 1990; Sanford, 2001b), the latter two raking kinematic components will, in synchrony, cause an opposing shearing motion of the TBA upper and lower jaws during the raking power stroke.

All linear measurements were calibrated using the background reference grid, and angular measurements were extracted so that an increase in angle reflects elevation of the structure. Linear and angular measurements were subtracted from their value at t_0 (cranial elevation onset) to facilitate direct comparison, except for gape distance, which was not reset to zero at t_0 to retain important information regarding mandibular jaw position prior to raking.

Derived variables

For each kinematic variable (Fig. 4), two derived variables were calculated, namely the magnitude of peak displacement after t_0, and the time (in ms) from t_0 to peak displacement. Since raking taxa generally occlude their jaws during raking (Sanford and Lauder, 1990; Sanford, 2001a; Sanford, 2001b), the peak gape displacement was actually when the predator's gape was the smallest distance. Peak hyoid displacement reflects maximum hyoid elevation, since the basihyal tooth plate is embedded into the prey item during raking. Peak cranial elevation was measured when the head and lower jaw were fully elevated during the rake (Fig. 2). The temporal variables were the corresponding time-to-peak values for each of the four displacement variables. Extraction of data for the outgroup analysis of raking kinematics, relative to strikes and chews from the ingroup and outgroup taxa, was performed following previous methods (Sanford, 2001b).

Statistical analyses

Descriptive statistics, including means and standard error for all eight raking variables, were calculated (Table 2). To evaluate the overall kinematic pattern of several variables, we used a principal component analysis (PCA) on the correlation matrix, with PC axes constrained to four, the eigenvalues of which exceeded 1. To examine overall inter-specific differences in raking behaviors, we ran a multivariate analysis of variance (MANOVA) on the PCA scores, with 'species' as a fixed effect and 'individuals nested within species' as a random effect. F-ratios for the main effect of species were tested using the mean square of individuals nested within species as the denominator

(Zar, 1999). A scatter-plot of the informative principal component axes (Fig. 5) was used to delineate the taxon distribution, relative to kinematic differences. Eigenvector-plotting of significant component loadings (>0.6) (Table 3), scaled to PC axis length, illustrates how the variables influenced differentiation of raking behaviors across multivariate kinematic space.

The outgroup analysis only differed in that the overall MANOVA used 'behavior' as a fixed effect. *F*-ratios for the main effect of behavior were tested using the error mean square as the denominator. A significant effect of behavior would suggest that the behaviors are different irrespective of taxon. Finally, *post-hoc* tests using Bonferroni-corrected pairwise comparisons were used to determine if raking was distinct from both the strike and chewing behaviors.

RESULTS

TBA morphology in *O. mykiss*

Osteology and myology of salmonid crania have been well studied (Greene and Greene, 1913; Norden, 1961; Rosen, 1974; Stearley and Smith, 1993; Sanford, 2000) and the following description therefore focuses on morphology directly comprising the TBA.

Mandibular jaws and the adductor mandibulae muscle

The upper oral jaws consist of a fixed premaxilla (Fig. 3A) and a posteroventrally tapering blade-like maxilla (not shown), both bearing single rows of stout caniniform dentition. In resting position, the non-protrusible mandible (Fig. 3B) lies parallel with the body axis. It bears similar canine-like dentition and articulates far posterior with the quadrate bone. Immediately anterior to this articulation, the prominent m. adductor mandibulae (AM) inserts on the medial face of the dentary *via* a single tendon, permitting AM contraction to rapidly close and immobilize prey between the oral jaws.

TBA jaws and protractor hyoideus muscle

Inside the oral cavity, the upper TBA is formed by lateral dentition on the dermopalatine (Fig. 3B), which is ankylosed to the suspensorium yet loosely associated with the premaxilla, maxilla and lateral ethmoid. This association allows the stout dermopalatine tooth row to remain embedded in the prey whilst allowing some lateromedial oral and buccal cavity kinesis during feeding. Further medial, the primary TBA teeth occupy the anteroventral vomerine surface and extend down the vomerine shaft (Fig. 3A) with an anteroventrally directed tooth curvature serving to effectively impale prey as it enters the oral cavity. In direct apposition are 6–8 posterior-curved fangs on a short and robust basihyal, which has a hinged articulation with the hypohyals allowing it to rotate dorsoventrally. The hyoid bar is composed of a large anterior and posterior ceratohyal, interconnected synarthritically by cartilage (Fig. 3B), their lateral faces providing the posterior attachment site for the anteriorly tapering protractor hyoideus muscle, which runs anteriorly to its attachment onto the distal-most mandibular ramus. The hyoid bar is flexibly attached to the distal hyomandible *via* the stout and short (~2 mm) interhyal.

Posterior neurocranium and epaxial musculature

The neurocranium (Fig. 3A) has a deep and robust supraoccipital crest with a deep anterior-directed fossa for epaxialis muscle insertion. With the cranial–vertebral joint located far ventrally at the cranial base, epaxialis muscle contraction will effectively rotate the neurocranium dorsally, bringing prey impaled on the vomerine dentition forward, relative to the ventral TBA (basihyal) teeth.

Pectoral girdle and hypaxial musculature

Points of flexion exist between the supraoccipital crest and the posttemporal, supracleithral and cleithral bones of the pectoral girdle. In conjunction, these points of flexion facilitate anteroposterior, and also dorsoventral, mobility of the large cleithrum but are obscured from the view of the camera by the operculum. Therefore, manipulations of anesthetized as well as unfixed specimens were used to estimate this dorsoventral pectoral girdle, or intra-pectoral flexion, to approx. 25 deg. (Fig. 3). Further distal on the girdle, the cleithrum is ankylosed with the keel-shaped coracoid, which meets its antimere in the midline. The posterior ramus of the coracoid provides a surface for hypaxialis insertion and space for pectoral fin musculature. Hypaxialis shortening will rotate the ventral pectoral girdle caudally and retract the basihyal *via* the SH muscle and cleithrobranchial ligament.

Sternohyoideus muscle and cleithrobranchial ligament

The paired SH muscle originates on the anterior coracoid face and inserts onto a large, leaf-shaped urohyal that is attached anteriorly *via* a stout ligament to the ventral hypohyal on each side. A prominent bilateral, CBL is embedded within the SH, originating at the medial anterior tips of the coracoid pair and extending anterodorsally towards the basihyal series (Fig. 3A). Here, each ligament partially attaches to a ventral cartilaginous tip of the third hypobranchial, which has become re-orientated relative to the more horizontal hypobranchial 1 and 2 (for clarity, not shown in Fig. 3A). From here, a major portion of the ligament then extends directly anterior and inserts onto the ventral aspect of the first basibranchial, resulting in an arc-shaped CBL shape.

TBA morphology in *S. jardinii*

Osteoglossid cranial morphology has previously been described extensively (Greenwood, 1971; Greenwood, 1973; Hilton, 2003) and herein we present only those traits (Fig. 3C) that vary from *O. mykiss* (see above).

Table 3. PC loadings from a principal component analysis comparing raking kinematics in *O. mykiss* and *S. jardinii*

	PC1	PC2	PC3	PC4
	28%	20%	15%	13%
Kinematic variables	Component loadings			
Cranial elevation timing	0.860	0.140	–0.108	–0.055
Hyoid distance timing	0.834	–0.247	0.012	0.006
Pectoral girdle retraction timing	0.530	**0.658**	0.106	0.244
Hyoid elevation amplitude	0.513	–0.185	**0.618**	0.264
Pectoral girdle retraction amplitude	–0.208	**0.870**	0.047	0.174
Gape distance timing	0.256	0.362	**–0.615**	–0.205
Cranial elevation amplitude	–0.283	0.368	**0.606**	–0.247
Gape distance amplitude	0.233	0.102	0.206	–0.872
Univariate *F*-statistics (d.f.=1, 3)	6.353	11.123	21.051	3.614
	P>0.05	*P*<0.05	*P*<0.01	*P*>0.05

Individual variance was factored out using a mixed-model ANOVA. Bold PC loadings (values >0.6) are plotted as eigenvectors in Fig. 5.

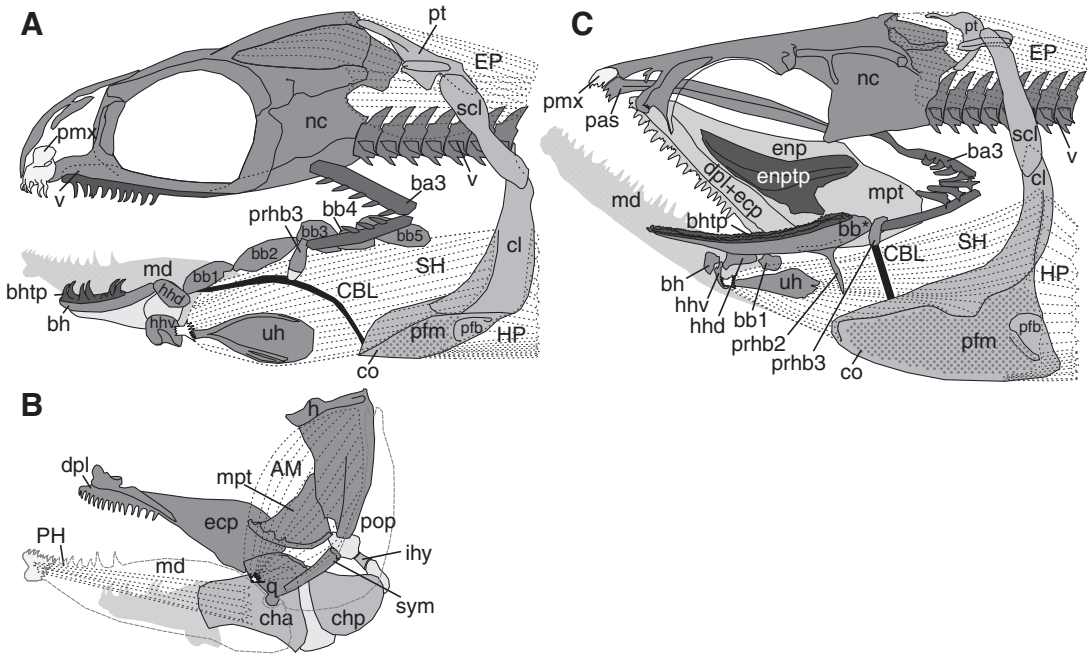

Fig. 3. Diagrammatic illustration of tongue-bite apparatus (TBA) in salmonid and osteoglossomorph fishes showing (A) medial TBA components and musculature driving the power stroke in *O. mykiss*, (B) left lateral components of the TBA and musculature involved in the preparatory phase of raking in *O. mykiss* and (C) medial TBA components and musculature driving the power stroke in *S. jardinii*. In A and C, the darkest grey indicates the directly opposed TBA dentition relevant to this study. In B, the left lateral mandible and preoperculum bones are only outlined to expose medial structures; the lateral-most of which is the dark-shaded suspensorium. Muscle and bone labeling is derived from Rosen, Sanford and Hilton (Rosen, 1974; Sanford, 2000; Hilton, 2003). Muscles: SH, m. sternohyoideus; PH, m. protractor hyoideus; AM, m. adductor mandibularis; EP, m. epaxialis; HP, m. hypaxialis. Ligaments: CBL, cleithrobranchial ligament; LAM, ligament of the AM inserting onto the mandible; LSH, ligament of the SH inserting onto the hyoid. Bones: ba3, 3rd branchial arch; bb1–5, basibranchials 1–5; bb*, fused basibranchial 2–5, forming the basihyal tooth plate foundation; bh; basihyal; bhtp, basihyal tooth plate; cha, anterior ceratohyal; chp, posterior ceratohyal; cl, cleithrum; co, coracoid; dpl, dermopalatine; ecp, ectopterygoid; enp, endopterygoid; enptp, endopterygoid tooth plate; hhd, dorsal hypohyal; hhv, ventral hypohyal; h, hyomandible; ihy, interhyal; m, mandible; mpt, metapterygoid; nc, neurocranium; pas, parasphenoid; pop, preoperculum; pmx, premaxilla; pfb, pectoral fin base; pfm, pectoral fin muscle; prhb2, process on 2nd hypobranchial; prhb3, process on 3rd hypobranchial; pt, posttemporal; q, quadrate; s, symplectic; scl, supracleithrum; uh, urohyal; v, vertebral column.

Mandibular jaws

The mandible in *S. jardinii* is longer and delineates a lateromedially compressed oral cavity and a distinct trap-door mouth with a dorso-oblique incline (Fig. 2). Both mandible and maxilla have correspondingly longer rows of caniniform dentition.

TBA jaws and protractor hyoideus muscle

The elongation of oral dentition rows transform to dentition on the dermopalatine and the suspensorium, which is tightly associated with the neurocranium, both at the ethmoid and sphenoid regions. Upper medial TBA dentition is restricted to two separate sets of caniniform teeth on the anterior and posterior-most ventral parasphenoid. Meanwhile, extensive stout papilliform dentition forms a tooth plate on the medial endopterygoid face. Correspondingly, a long and slender tooth plate with dense papilliform dentition overlies the basihyal, dorsal hypohyal and basibranchials 1–3, while the basihyal–ceratohyal–interhyal–hyomandibular series resembles the series in *O. mykiss*.

Post-cranial morphology

The supraoccipital crest is low-rising and narrow with a shallow fossa providing restricted insertion space for the epaxialis musculature, segments of which also insert onto the posttemporal and supracleithral bones. While the pectoral girdle has the same articulations as in *O. mykiss*, manipulations showed that intra-pectoral flexion was less pronounced (10±2 deg.), yet the ventral girdle provides larger surfaces for posterior hypaxialis and anterior SH attachment than in *O. mykiss*.

Sternohyoideus muscle and cleithrobranchial ligament

The SH muscle is relatively slender and tapers off towards the anterior insertion onto a small sesamoid urohyal. While the cleithrobranchial ligament originates bilaterally at locations similar to those in *O. mykiss*, the ligament is more robust in *S. jardinii* and inserts entirely onto a bony process of the third hypobranchial and not onto the prominent styloid process of the second hypobranchial (Hilton, 2001), which forms an attachment site for at least some SH muscle fibers.

Raking kinematics

Raking is initiated with a preparatory phase at –30 ms in *O. mykiss* (Movie 1 in supplementary material) and at –70 ms in *S. jardinii* (Movie 2 in supplementary material), with abrupt mandibular jaw occlusion (Fig. 2A,G). In *S. jardinii*, distinct and unique cranial depression kinematics (Fig. 2H; Fig. 3C), in conjunction with pectoral girdle protraction (Fig. 2H; Fig. 3D), also begins early at –70 to –30 ms. The lower jaw is elevated prior to t_0, followed by depression, which starts and peaks earliest in *O. mykiss.* The externally visible hyoid motion (point 8 in Fig. 2A,G; Fig. 4B) appears minimal in both taxa (~0.1 cm; Table 2); however, prior to t_0, a detectable gradual elevation of the hyoid in *S. jardinii* ends at the onset of the power stroke (t_0) (Fig. 2H; Fig. 4B). The raking

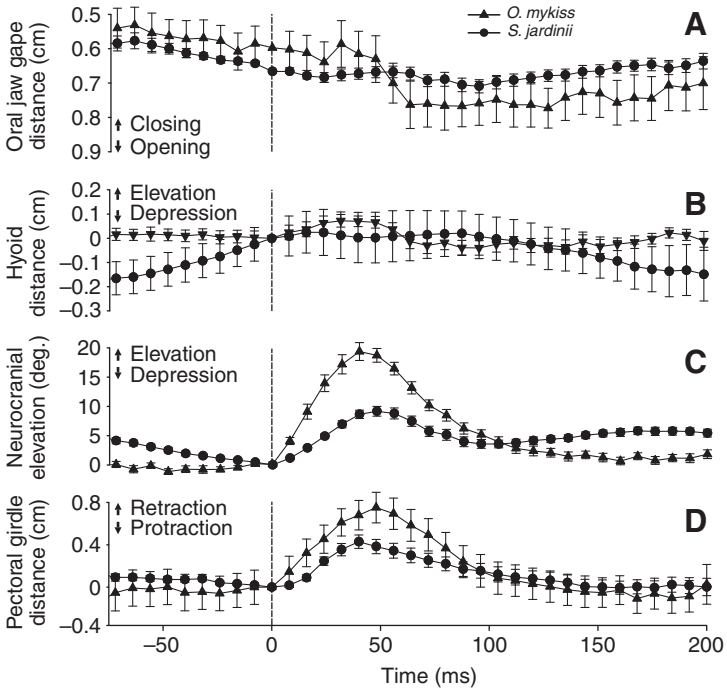

Fig. 4. Mean profile plots for four derived kinematic variables during raking on goldfish prey in *O. mykiss* and *S. jardinii*. (A) Gape distance excursion; (B) hyoid distance; (C) cranial elevation; (D) pectoral girdle retraction. Triangles, *O. mykiss*; circles, *S. jardinii*. t_0=onset of cranial elevation. Note that jaw adduction remains constant in *S. jardinii* while in *O. mykiss* hyoid movements are more pronounced.

power stroke begins with the onset of cranial elevation (t_0) (Fig. 2B,I; Fig. 4D) and is accompanied in both taxa by the onset of pectoral girdle retraction. Both cranial elevation and pectoral girdle retraction in *O. mykiss* are approximately double that in *S. jardinii* (Table 2). Interestingly, maximum cranial elevation and pectoral girdle retraction occur at approximately the same time (44 ms) in *O. mykiss*, while in *S. jardinii* maximum cranial elevation occurs after maximum pectoral girdle retraction (50±2.55 ms and 38±5.17 ms, respectively). Overall, cranial and pectoral girdle movements are greater and (with the exception of the pectoral girdle) faster in *O. mykiss* (Fig. 4; Table 2) while the raking preparatory phase in *S. jardinii* is more complex.

A PCA on the correlation matrix from the kinematic dataset returned four axes with eigenvalues exceeding one, together explaining 76% of the dataset variance (28%, 20%, 15% and 13%, respectively). While a MANOVA found overall significant differences in the dataset (Wilk's λ=0.227; $F_{4,30}$=25.527; P<0.001), a significant species effect was only evident along axes PC2 and PC3, accounting for a total of 28% of the variation (Table 3). Five of the eight kinematic variables along these axes had component loadings over 0.6 (Table 3), indicating that they were influential in taxon separation. Nevertheless, a scatter plot of PC2 and PC3 (Fig. 5) shows extensive species polygon overlap in multidimensional kinematic space. The spread of cases in this plot also shows that raking behaviors in *S. jardinii* are more variable while raking is more stereotypical in *O. mykiss*. Cranial elevation amplitude loaded significantly along PC3, being almost double in *O. mykiss* (22.41±1.62 deg.) compared with *S. jardinii* (13.05±1.45 deg.) (Fig. 4; Tables 2 and 3), as well as reaching a peak earlier in *O. mykiss* than in *S. jardinii* (Table 2). Pectoral girdle retraction was much greater but peaked later in *O. mykiss* than in *S. jardinii* (7.5 mm and 44.3 s *vs* 4.1 mm and 38.2 ms). Despite minimal hyoid movements in both taxa, hyoid elevation was more prominent in *S. jardinii* during almost the entire raking behavior (Fig. 4), and minimum gape distance occurred significantly later in *S. jardinii* (Table 2). It is noted, however, that the latter two variables exerted less influence on taxon segregation than the first three, as indicated by their vector planes being perpendicular to the major segregation axis of species polygons in Fig. 5.

General feeding kinematics

A PCA on the correlation matrix of a dataset including strike and chewing kinematics from all four taxa and raking kinematics from the ingroups recovered three PC axes with eigenvalues exceeding one, which explained 39%, 26% and 13% of the total dataset

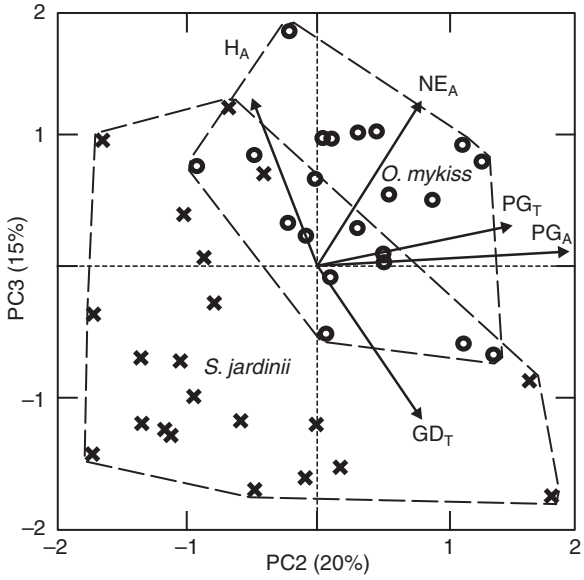

Fig. 5. Scatter plot of PC2 and PC3 from a principal component analysis on kinematic timing and magnitude data (Table 2) associated with *O. mykiss* and *S. jardinii* raking. Eigenvectors represent significant component loading values (Table 3), scaled to PC1 axis length, for the following variables: NE_A, cranial elevation amplitude; PG_A, pectoral girdle retraction amplitude; PG_T, pectoral girdle retraction timing; H_A, hyoid distance amplitude; GD_T, gape distance timing.

variance, respectively. A MANOVA recovered statistically significant behavioral differences in the dataset (Wilk's λ=0.201; $F_{16,126}$=9.692; P<0.001). Subsequent ANOVAs on the PC factor scores revealed that all axes contained statistically significant differences in behavior ($F_{2,75}$=13.793, 6.686 and 16.045 for PC1–3, respectively; all at P<0.001). Along PC1, raking separated from chewing (P<0.001) but not from strikes (P=0.762), driven by an earlier time to peak in all kinematic displacements (Fig. 6). Increased amplitude of hyoid, mandibular and pectoral girdle motion separated raking from chewing (P<0.05) but not from strikes (P=0.053) along PC2, while increased cranial elevation drove raking from other behaviors (P<0.001) and chewing from strikes (P<0.05) along PC3 (Fig. 6). Raking thus differed significantly from at least one of the other behaviors along all informative PC axes.

Raking biomechanical models

In both taxa, the raking preparatory phase involves two musculoskeletal events. Concomitant mandibular jaw occlusion and basihyal protraction immobilizes the prey between the mandibular and TBA jaws (Fig. 2) and effectively 'charges' the TBA for the power stroke (Fig. 7A,B). Mandibular jaw occlusion is rigorously maintained throughout the rake, and, after the preparatory phase, the raking power stroke may be accomplished by a combination of the following biomechanical mechanisms, which are discussed in detail below (see also Movie 3 in supplementary material): (1) anterodorsally directed rotation of the dorsal TBA jaw *via* cranial elevation (Fig. 7C,D); (2) posterior excursion of the basihyal *via* two complementary musculoskeletal pathways – (a) indirectly *via* hypaxialis-driven pectoral girdle retraction (Fig. 7E,F) and (b) directly, *via* sternohyoideus contraction (Fig. 7G,H).

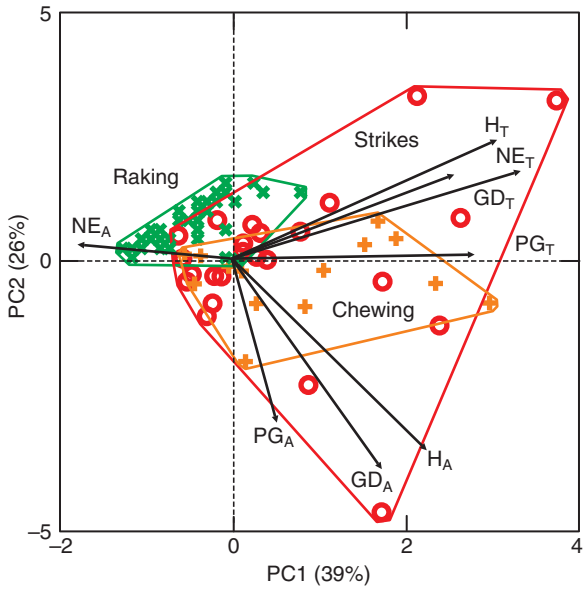

Fig. 6. Scatter plot of PC1 and PC2 from a principal component analysis on kinematic timing and magnitude data (Table 2) associated with behaviors: raking (green crosses) in *O. mykiss* and *S. jardinii*, and chewing (orange crosses) and strikes (red circles) in all taxa. Eigenvectors as in Fig. 5. NE_A, cranial elevation amplitude; NE_T, cranial elevation timing; H_A, hyoid distance amplitude; H_T, hyoid distance timing; PG_A, pectoral girdle retraction amplitude; PG_T, pectoral girdle retraction timing; GD_A, gape distance amplitude; GD_T, gape distance timing. Note that while cranial elevation amplitude loaded most strongly along PC3 (not shown), its vector plane was identical to that shown in the PC1–2 plot.

DISCUSSION

TBA morphology and raking kinematics

We provide the first comparative analysis of morphology and kinematics in taxon representatives from two unrelated lineages that have a novel tongue-bite apparatus (TBA) and use a derived raking behavior during prey-processing (Sanford and Lauder, 1989; Ishiguro et al., 2003). Below, we synthesize the interspecific similarities and differences in TBA morphology and raking kinematics with available muscle activity evidence (Konow and Sanford, 2008) and discuss the implications to our biomechanical hypotheses for TBA function during raking.

Clear similarities in TBA gross morphology existed in *O. mykiss* and *S. jardinii*, including the presence of (1) basihyal dentition, (2) opposing dentition in the oral cavity roof and (3) a cleithrobranchial ligament (CBL). Dentition on various bone surfaces inside the oral and anterior buccal cavity is a basal trait in teleosts (Hilton, 2001). Thus, the convergent evolution of a CBL and associated hypertrophy of basihyal and opposing mouth roof dentition appears to be an example of an 'evolutionarily stable configuration' (Schwenk and Wagner, 2000; Wagner and Schwenk, 2000). Despite the convergent TBA morphology, these traits differed qualitatively between taxa, in (1) TBA upper jaw dentition distribution, (2) dentition morphology in the TBA jaws and (3) different origin-insertion paths of the CBL. This supports earlier notions that the TBA is a character suite and not a single trait (Hilton, 2001), and the morphological differences emphasize that TBAs are not unambiguous inter-lineage convergent traits (Sanford, 2001b).

Strongly convergent trends were also evident in raking kinematics, including a gross behavioral sequencing into distinct, successive compressive preparatory, excursive power-stroke and expansive recovery phases (Sanford, 2001b). Raking kinematics involved concomitant cranial elevation and pectoral girdle retraction during the power stroke in both taxa, which is also a ubiquitous suction-feeding characteristic. During raking, pectoral girdle retraction is notably amplified compared with other feeding behaviors and is coupled with a novel preparatory hyoid protraction and early jaw occlusion, maintained to different extents in each taxon throughout the power stroke. Therefore, rather than resulting from entirely novel skull kinematics, our results suggest that raking is governed by a combination of derived kinematics (amplified pectoral girdle retraction, hyoid protraction followed by retraction). Meanwhile, the convergent changes in timing of the mandible, cranium and pectoral girdle motion during raking are relatively slight modifications of more basal aquatic behaviors, such as ventilation (Liem, 1984; Liem, 1985), prey capture (Lauder, 1985; Carroll, 2004) and prey-processing (Sibbing, 1982). Sampling of one taxon representative from each lineage is not conclusive evidence that raking between all the members of each lineage is convergent. Nevertheless, based on the morphology of the TBA among other representatives of these two lineages (Konow et al., 2008) and previous kinematic evidence (Sanford, 2001a; Sanford, 2001b), we propose a biomechanical model to be used to quantitatively evaluate the level of raking convergence between multiple taxa from each lineage.

The input kinematic excursions in *O. mykiss* (neurocranial elevation, 22.41±1.23 deg.; pectoral girdle retraction, 0.75±0.06 cm) were less pronounced than in *Salvelinus fontinalis* (38.6±1.1 deg.; 0.83±0.06 cm), the only salmonid for which raking kinematics were previously presented (Sanford, 2001b; Konow et al., 2008). Moreover, *S. jardinii* displayed reduced neurocranial elevation (13.05±1.01 deg.) and amplified pectoral girdle retraction (0.41±0.13 cm) compared with *Osteoglossum bichirrosum* (ne: 26,

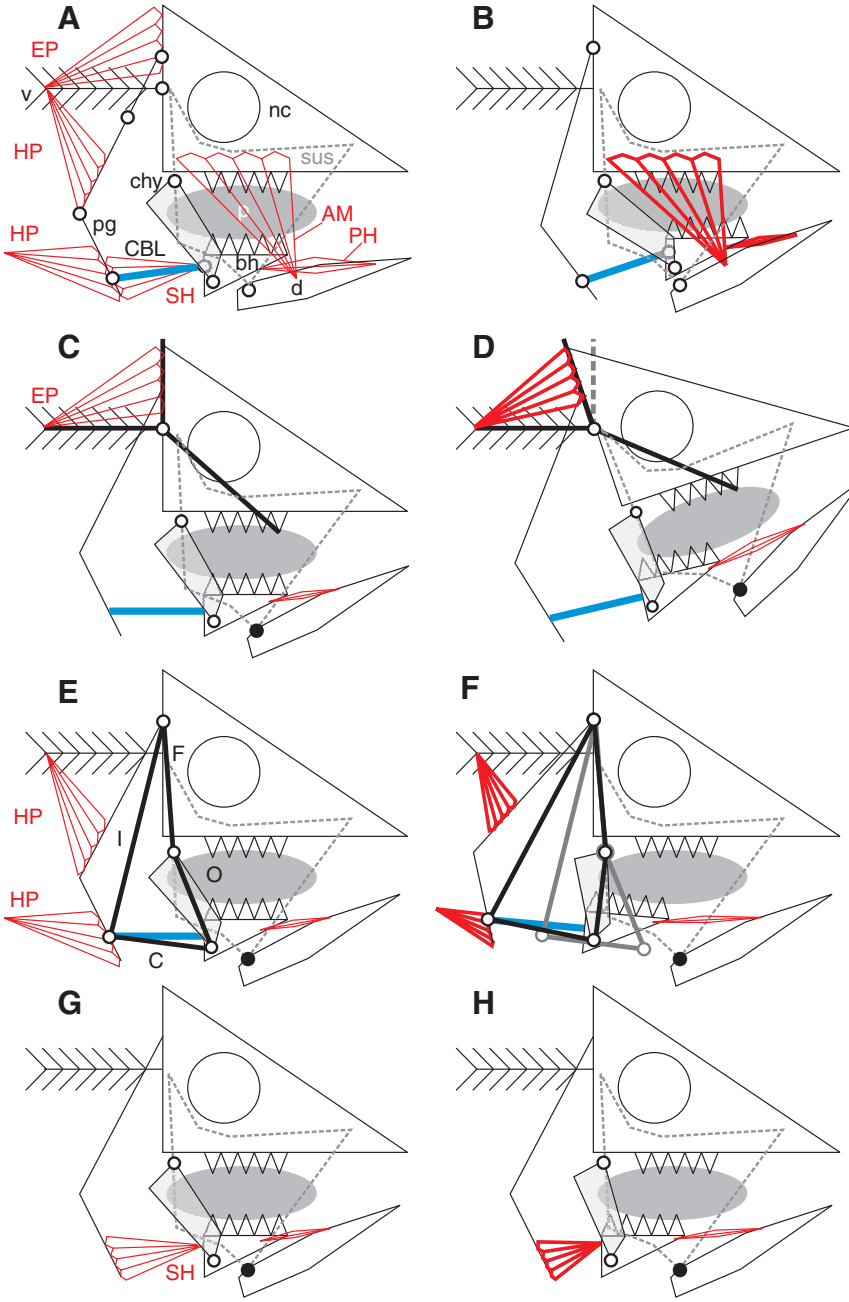

Fig. 7. Biomechanical models of cranial structures directly involved in raking, developed using morphological and kinematic evidence from *O. mykiss* and *S. jardinii*. Muscles are indicated with red lines, heavy when muscle contraction is inferred. (A,B) Raking preparatory phase, involving basihyal protraction, elicited by the PH muscle, and lower jaw occlusion, elicited by AM contraction. Three raking power-stroke pathways were derived from results in this and previous studies: (C,D) cranial elevation elicited by EP muscle contraction (with the BH anchored by the CBL to the cleithrum, held fixed by HP and/or regionally specialized EP musculature) and explained by a third-order lever system (black bars; heavy grey broken line in D indicates the initial position of this lever); (E,F) pectoral girdle retraction elicited by HP muscle contraction [the CBL (blue) and SH linking pectoral girdle and BH] described by a planar four-bar linkage [black quadrilateral; I, input linkage (EP); F, fixed lever (neurocranium); O, opening lever (TBA gape); C, coupler linkage (CBL and SH) (heavy grey broken quadrilateral in F indicates the initial position of this linkage)]; (G,H) basihyal retraction directly elicited by SH contraction (where the CBL plays no direct role). Abbreviations: SH, m. sternohyoideus; PH, m. protractor hyoideus; AM, m. adductor mandibularis; EP, m. epaxialis; HP, m. hypaxialis; CBL, cleithrobranchial ligament; nc, neurocranium; chy, ceratohyal; pg, pectoral girdle; sus, suspensorium; bh, basihyal; v, vertebral column; d, dentary; p, prey.

27±1.6 deg.; pg: 0.22±0.02 cm), an osteoglossid sister taxon (Sanford and Lauder, 1990), but much less neurocranial elevation than in the notopterid *Xenomystus nigri* (34.7±1.03 deg.) (Sanford, 2001a). Thus, raking kinematics in the study taxa presented here were not as similar as predicted, based on evidence from their close sister taxa, corroborating Sanford's finding that considerable kinematic differences can exist in raking kinematics (Sanford, 2001a) despite close phylogenetic position and similar TBA morphology (Taverne, 1979). This further suggests that even subtle differences in muscle activity and recruitment can result in functionally divergent raking kinematics (Sanford, 2001a). An interesting future avenue of research would be to compare the relative magnitude of contribution from neurocranial and pectoral girdle input kinematics to basihyal output kinematics during the power stroke.

Our results suggest that, although raking behaviors are generally driven by the same input kinematics in both lineages, subtle interspecific differences are also present, namely in the magnitude of cranial elevation and pectoral girdle kinesis. Meanwhile, timing variables are less influential on taxon segregation, which may indicate that (1) raking is governed by tight neuro-motor control, suggesting temporal stereotypy (e.g. Alfaro et al., 2001; Ross et al., 2007), and (2) behavioral modulation, and not interspecific differences in one or both taxa, results in the observed differences in power-stroke excursion magnitudes (Konow et al., 2008).

The more variable raking kinematics in *S. jardinii* compared with *O. mykiss* (Fig. 5) correspond well with muscle activity differences between these taxa, involving convergence of AM and m. protractor hyoideus (PH) activity during the preparatory phase and diversity in SH, m. hypaxialis (HP) and m. epaxialis activity during the power-stroke phase [see fig. 5 in Konow and Sanford (Konow and Sanford, 2008)]. Thus, while raking relies on a convergently derived shift in musculoskeletal function, subsequent diversification in raking

kinematics may have occurred (Sanford and Lauder, 1990; Sanford, 2001a).

For example, our data suggest that osteoglossid raking kinematics is more complex than a previous analysis of *Osteoglossum bicirrhosum* revealed (Sanford and Lauder, 1990). Notable cranial depression and subtle pectoral girdle protraction occur during the raking preparatory phase in *S. jardinii*, presumably augmenting basihyal protraction relative to the TBA upper jaw. This preparatory protraction increases the distance that the basihyal moves when retracted during the power stroke, an augmented TBA 'priming' that may explain the restricted cranial elevation and pectoral girdle retraction in *S. jardinii* compared with *O. mykiss*, which does not display such extensive preparatory kinesis. Moreover, pronounced hyoid elevation and firmer mandibular jaw occlusion in *S. jardinii* suggest that compressive forces onto the prey are achieved, which may reduce the need for the extensive neurocranial and pectoral girdle power-stroke excursions commonly seen in other raking taxa (Lauder and Liem, 1983; Sanford and Lauder, 1989).

Compressive raking kinematics in *S. jardinii* may interplay with morphological specializations, which involve a rigid oral cavity roof with a chevron-shaped cross section and a lateral profile that is anterodorsally inclining [see also fig. 2 in Sanford and Lauder (Sanford and Lauder, 1990)]. The millstone-like TBA tooth plates are thus angled at 45 deg. relative to the body axis in *S. jardinii* whereas the tooth plates in *O. mykiss* are parallel to the body axis (Fig. 3). Differences in CBL morphology may be a key component in altering the transmission efficiency of hypaxial strain into basihyal power-stroke kinesis. A straight CBL may theoretically deliver a more direct and rapid hypaxial strain transmission in *S. jardinii*. An arc-shaped ligament, on the other hand, may explain the faster and amplified cranial and pectoral girdle kinematics in *O. mykiss*, which act to straighten the CBL in order to achieve powerful posteriorly directed basihyal raking motion. Alternatively, amplified power-stroke kinematics may not only serve to reduce hard prey but also to immobilize more elusive naturally selected prey, a function that future studies of modulation in response to different prey types may answer (Sanford, 2001b; Konow et al., 2008).

Intra-pectoral flexion, *via* articulations between the coracoid, cleithral, supracleithral and postcleithral girdle elements, is another potentially important and hitherto unexamined variable. Specimen manipulations revealed inter-specific differences in intra-pectoral flexion, which in both study taxa exceeded values for taxa presented by Muller (Muller, 1987). Associated kinematic differences, if present, remain unquantified, as the pectoral girdle is largely obscured by the operculum in live specimens. However, high-speed videos of one *S. jardinii* specimen with eroded operculi have revealed that there is some rotational movement between the posttemporal and supracleithrum, which may be facilitated by epaxial regional specialization (Thys, 1997; Carroll, 2004). Basal teleosts lack a protractor pectoralis (Greenwood and Lauder, 1981), yet the fiber orientation of other deep muscles, e.g. the obliquus superioris, pharyngocleithrals internus or p. externus, may permit such complex pectoral girdle kinesis [see fig. 7 in Lauder and Liem (Lauder and Liem, 1980)].

Is raking a convergently derived behavior?

Quantitative comparisons of raking in the representative ingroups (osteoglossomorphs and salmonids) with other behaviors existing in both ingroups and outgroups (*Esox* and *Amia*) provide strong support for the hypothesis that raking is convergently derived in the two TBA-bearing lineages. Coupled with the changes in morphology discussed above, raking results from a convergently derived shift in the muscle activity pattern; specifically, an early onset occurs in hyoid protractor and mandibular adductor muscles (Konow and Sanford, 2008). This novel MAP yields the differences in phase sequencing between the examined feeding behaviors (Table 1B). Our results also suggest that rakes differed more from chews than strikes and, indeed, raking could be a functional derivative of a 'closed-mouth strike'. Raking also differed from both chews and strikes by having a more pronounced pectoral girdle kinesis and from strikes by gape closing and hyoid elevation movement during the power strokes of the respective behaviors. During raking there is extensive pectoral girdle retraction, and the limited dorsoventral movement of the basihyal suggests that it is moving primarily anteroposteriorly during the power stroke. Sonomicrometry data from other taxa, including raking taxa, suggest that basihyal output kinematics may be partly obscured using external landmarks (Sanford and Wainwright, 2002; Konow et al., 2008). However, it is clear from the present study that the derived variables all loaded heavily along statistically informative PC axes and described three input kinematic mechanisms for modeling of the raking power stroke.

TBA biomechanical models

The musculoskeletal configuration of the TBA and the temporal sequence of raking indicate that this system primarily functions in an anteroposterior direction in the midsagittal plane, as confirmed in ventral view. Moreover, the externally visible kinematics of the mandible, neurocranium and pectoral girdle suggests that the input mechanisms function synergistically. Using the data presented herein, and based on modifications to existing four-bar linkage and third-order lever models (Muller, 1987; Carroll, 2004; van Wassenbergh et al., 2005), we propose three complementary and synergistic component models for raking biomechanics (Fig. 7). The models will aid future quantifications of the relative contribution of each to the overall raking pattern both within and between taxa (Wainwright et al., 2004; Grubich and Westneat, 2006). Future multi-taxon analyses may empirically calibrate the models and determine if these input mechanisms synergistically result in functional many-to-one mapping (Alfaro et al., 2005).

Component models

As outlined above, the raking preparatory phase involves protraction of the basihyal and occlusion of the mandibular jaws (Fig. 7A,B). The role of cranial elevation during the subsequent raking power stroke differs from its role during, for example, strikes (Fig. 7C,D), while still functioning as a third-order lever (Carroll, 2004; Carroll and Wainwright, 2006). During strikes, epaxial shortening causes cranial elevation, which drives inter-opercular rotation, maxillary rotation, jaw protrusion and/or hyoid depression (Anker, 1974; Motta, 1984; Muller, 1987; Muller, 1989; Westneat, 1991). However, since all these output kinematics during raking are impeded by jaw occlusion, cranial elevation instead causes anterior displacement of the TBA upper jaw from the posteriorly moving lower (basihyal) jaw (Fig. 7E,F).

During the raking power stroke, TBA gape distance is maintained relatively constant, as indicated by the ~0.1–0.2 cm dorsoventral hyoid excursion measured in both taxa. Mandibular jaw motion was also relatively restricted in both taxa (0.1 cm in *S. jardinii*; 0.2 cm in *O. mykiss*) and did not contribute statistically to taxon separation. Dorsoventral compression of the TBA is augmented throughout the power stroke by maintained mandibular jaw occlusion in both taxa. Moreover, the prolonged PH contraction in *S. jardinii* further

impedes posteriorly directed hyoid excursion (Konow and Sanford, 2008). While pronounced variation exists in other raking input kinematics, occluded mandibular jaws during the raking power stroke appear to be a ubiquitous trait (Sanford and Lauder, 1989; Sanford and Lauder, 1990; Sanford, 2001a). Thus, dorsoventral TBA compression may contribute to an efficient raking power stroke.

We model hypaxial strain transmission during the raking power stroke, *via* the pectoral girdle and sternohyoideus–cleithrobranchial ligament (SH–CBL) complex to basihyal retraction, using a four-bar planar linkage model (Fig. 7E,F). The model builds on the four-bar links in Muller's hyoid depression model (Muller, 1987); however, in our model, the 'fixed link' is the distance from the interhyal–symplectic joint, *via* the hyomandible and neurocranium, to the posttemporal–supracleithral joint (i.e. Muller's input link). At this joint, the pectoral girdle 'input link' (Muller's fixed link) articulates with the neurocranium. The 'coupler link' extends from the CBL origin on the ventromedial pectoral girdle, *via* the SH–CBL complex, to the ceratohyal–basihyal joint (Muller's output link), from where the anterior and posterior ceratohyal 'output link' connects, *via* a short and stout interhyal, onto the suspensorium (Muller's coupler link).

Uncertainties regarding the validity of the proposed model as well as existing four-bar linkage models (including Muller's model) are addressed in detail below.

(1) Fixed-link deviation from 2-D may be less pronounced in raking taxa, despite the presence of interhyal articulations, as the hyomandible is more robustly associated with the neurocranium *via* less flexible suspensoria than in most of the derived teleosts modeled by Muller (Muller, 1987).

(2) Input-link distortion results from intra-pectoral girdle flexion around the cleithrum–supracleithrum–posttemporal–occipital junctions, articulations that are generalized teleost traits, making the present model no more or less prone to error than Muller's model.

(3) Coupler link distortion potentially results from highly labile contractile patterns in the SH muscle during teleost feeding (van Wassenbergh et al., 2005; van Wassenbergh et al., 2007; Carroll, 2004). Isotonic contraction of the SH during raking will cause posteriorly directed basihyal retraction (Fig. 7G,H), while eccentric or absent SH contraction during HP-mediated pectoral girdle retraction will cause SH stretching, which in the case of *O. mykiss* will straighten the arc-shaped CBL. Sonomicrometry measurements from *O. mykiss* have shown that maximal SH stretching is restricted to approx 2% of SH resting length, a limitation that likely is explained by straightening of the arc-shaped CBL (Konow and Sanford, 2008). The PH mechanically antagonizes the basihyal retractor musculature (SH and HP). During the raking preparatory phase, we propose that PH shortening protracts the basihyal towards the mandibular symphysis, thereby maximizing the subsequent basihyal retraction during the power stroke. A maintained PH contraction during the power stroke, as observed in *S. jardinii*, mechanically prevents basihyal retraction, from which coupler-link stretching and basihyal elevation may result (Konow and Sanford, 2008). Moreover, maximal lower jaw depression, coupled with hyoid depression during strikes, may also result in straightening of the arc-shaped salmonid CBL, which only when straightened will be capable of direct force transmission from hypaxial musculature to the basihyal, functionally decoupling the SH. While the coupler link (Muller's output link) clearly is one of the more 'irregular' four-bar links, it is uniquely reinforced by a CBL in all raking teleosts (although absent in *Pantodon*) (Sanford and Lauder, 1990). The coupler link distortion that could result from the musculoskeletal dynamics in the ventral TBA may be at least partly mitigated by the presence of a straight CBL in osteoglossomorphs (Sanford and Lauder, 1989; Hilton, 2001; Konow and Sanford, 2008). This, however, assumes that the CBL is not an elastic structure, which is currently under investigation.

(4) Output link deviation from 2-D is a known issue given that the posterior margin of the ceratohyals flare laterally during buccal cavity expansion in suction feeding, *viz.* Muller's four-bar isosceles linkage (Muller, 1989), a pattern that has already been quantified *via* sonomicrometry (Sanford and Wainwright, 2002). However, this link describes both dorsoventrally curvilinear basihyal motion during strikes and chews and anteroposterior ellipsoid motion during rakes. Although flaring of the suspensorium means that the four-bar output link deviates from 2-D, some of this motion is absorbed by interhyal rotation, which permits the hyoid bar to initially shift posteriorly, like during suction feeding (De Visser and Barel, 1996). Flaring clearly diverges from the 2-D motions that can be explained by conventional engineering four-bar linkage theory. However, the discrepancies in output link length required to alter basihyal motion from curvilinear (Sanford and Wainwright, 2002) to ellipsoid are theoretically restricted to the freedom of motion around the interhyal, which connects the ceratohyal output link to the suspensorial fixed link (De Visser and Barel, 1996; Muller, 1996).

Testing and calibrating the four-bar model

The functional deviations from planar four-bar linkage theory outlined above are far from unprecedented examples of how four-bar models inaccurately quantify musculoskeletal systems. Nevertheless, four-bar models retain their usefulness by reducing organismal complexity to a level that is computationally more feasible and permits calculation of lever ratios and mechanical advantages [*viz.* Fig. 3 *vs* Fig. 7A and 7E,F; illustrating that the hyoid linkage proposed herein, and by Muller (Muller, 1987), in organismal reality is a '10-bar']. Interspecific differences were seen in all kinematic input mechanisms driving raking power strokes. Consequently, the model hypotheses presented herein will be important contributions in future comparative studies of raking, both within and between the phylogenetically unrelated raking lineages and across the organizational levels of morphology, muscle activity and kinematics (Muller, 1987). Detection of, and compensation for, link distortion or link 2-D deviations is possible using sonomicrometry (Sanford and Wainwright, 2002) or 3-D fluoroscopy (Brainerd et al., 2007), which may provide taxon-specific empirical data to calibrate the raking four-bar linkage. Currently, direct tests of biomechanical models in aquatic vertebrate feeding remain limited to volumetric expansion during suction feeding (Muller and Osse, 1984; Van Wassenbergh et al., 2006), sonomicrometric quantifications of hyoid depression in suction feeding (Sanford and Wainwright, 2002; Wilga and Sanford, 2008) and the effect of cranial elevation on suction-pressure generation (Carroll, 2004; Carroll and Wainwright, 2006). Few complete four-bar linkage models have undergone comprehensive empirical testing (van Wassenbergh et al., 2005; Roos et al., 2008), yet component links have been dynamically quantified [*viz*. the levator posterior muscle in a four-bar model of Grubich and Westneat (Grubich and Westneat, 2006)].

Basal and derived raking mechanisms

Basihyal elevation and protraction during the preparatory phase, combined with a power stroke driven by cranial elevation, is a conservative combination of raking input mechanisms in salmonids (Sanford, 2001b) (present study). This pattern also occurs in some osteoglossomorphs [*Osteoglossum* (Sanford and Lauder, 1990);

Xenomystus (Sanford, 2001a)], while other taxa mainly utilize pectoral girdle retraction (Sanford and Lauder, 1989). Analyses of *Hiodon*, the basal-most osteoglossomorph and extant raking taxon (Hilton, 2003; Lavoué and Sullivan, 2004), may confirm the ancestral input mechanisms. This would help determine whether salmonids use a basal or derived suite of input mechanisms and permit quantification of the evolutionary changes in input mechanisms within and among the raking lineages. Phylogenetic hypotheses and fossils are plentiful for both lineages and their relatives (Stiassny et al., 1996; Ishiguro et al., 2003). Time-calibrated analyses could thus yield robust tests of how different component mechanisms contribute to functional disparity. Such analyses would significantly improve our understanding of how evolutionary rates in the evolution of structural and functional disparity influence the differentiation of novel behaviors.

LIST OF SYMBOLS AND ABBREVIATIONS

AM	m. adductor mandibulae
CBL	cleithrobranchial ligament
EP	m. epaxialis
HL	head length
HP	m. hypaxialis
MAP	muscle activity pattern
PCA	principal components analysis
PH	m. protractor hyoideus
PJA	pharyngeal jaw apparatus
SH	m. sternohyoideus
t_0	raking power-stroke onset or 'time-zero'
TBA	tongue-bite apparatus

We thank A. Camp, M. Ajemian, M. McGuire and M. Kats for experiment assistance, Hofstra University Animal Care Facility staff for daily specimen maintenance, and P. Doherty, A. Camp and two anonymous reviewers for valuable comments on early manuscript drafts. This work was supported by the National Science Foundation (IOS#0444891, DBI#420440).

REFERENCES

Alfaro, M. E. and Herrel, A. (2001). Introduction: major issues of feeding motor control in vertebrates. *Am. Zool.* **41**, 1243-1247.
Alfaro, M. E., Janovetz, J. and Westneat, M. W. (2001). Motor control across trophic strategies: muscle activity of biting and suction feeding fishes. *Am. Zool.* **41**, 1266-1279.
Alfaro, M. E., Bolnick, D. I. and Wainwright, P. C. (2005). Evolutionary consequences of many-to-one mapping of jaw morphology to mechanics in labrid fishes. *Am. Nat.* **165**, 140-154.
Anker, G. C. (1974). Morphology and kinetics of the head of the stickleback, *Gasterosteus Aculeatus. Trans. Zool. Soc. Lond.* **32**, 311-416.
Brainerd, E. L., Gatesey, S. M., Baier, D. B. and Hedrick, T. L. (2007). Accurate 3D reconstruction of skeletal morphology and movement with CTX imaging. *J. Morph.* **268**, 1053.
Carroll, A. M. (2004). Muscle activation and strain during suction feeding in the largemouth bass, *Micropterus salmoides. J. Exp. Biol.* **207**, 983-991.
Carroll, A. M. and Wainwright, P. C. (2006). Muscle function and power output during suction feeding in largemouth bass, *Micropterus salmoides. Comp. Biochem. Physiol. A.* **143**, 389-399.
De Visser, J. and Barel, C. D. N. (1996). Architectonic constraints on the hyoid's optimal starting position for suction feeding of fish. *J. Morphol.* **228**, 1-18.
Dingerkus, G. and Uhler, L. D. (1977). Enzyme clearing of alcian blue stained whole small vertebrates for demonstration of cartilage. *Stain Technol.* **52**, 229-232.
Drucker, E. G. and Jensen, J. S. (1991). Functional analysis of a specialized prey processing behavior: winnowing by surfperches (*Teleostei: Embiotocidae*). *J. Morphol.* **210**, 267-287.
Ferry-Graham, L. A. and Lauder, G. V. (2001). Aquatic prey capture in ray-finned fishes: a century of progress and new directions. *J. Morphol.* **248**, 99-119.
Frost, B. J. and Sanford, C. P. J. (1999). Kinematics of a novel feeding mechanism in the osteoglossomorph fish *Chitala chitala*: is there a prey-type effect? *Zoology* **102**, 18-30.
Gillis, G. B. and Lauder, G. V. (1995). Kinemaitcs of feeding in bluegill sunfish: is there a general distinction between aquatic capture and transport behaviors? *J. Exp. Biol.* **198**, 709-720.
Greene, C. W. and Greene, C. H. (1913). The skeletal musculature of the king salmon. *Bull. U. S. Bureau Fish.* **33**, 21-60.
Greenwood, P. H. (1971). Hyoid and ventral gill arch musculature in osteoglossomorph fishes. *Bull. Br. Mus. Nat. Hist. Zool.* **22**, 1-55.
Greenwood, P. H. (1973). Interrelationships of osteoglossomorphs. In *Interrelationships of Fishes* (ed. P. H. Greenwood, R. S. Miles and C. Patterson), pp. 307-332. London: Academic Press.
Greenwood, P. H. and Lauder, G. V. (1981). The protractor pectoralis muscle and the classification of teleost fishes. *Bull. Br. Mus. Nat. Hist. Zool.* **41**, 213-234.
Grubich, J. R. (2003). Morphological convergence of pharyngeal jaw structure in durophagous perciform fish. *Biol. J. Linn. Soc. Lond.* **8**, 147-165.
Grubich, J. R. (2005). Disparity between feeding performance and predicted muscle strength in the pharyngeal musculature of black drum, *Pogonias cromis* (Sciaenidae). *Env. Biol. Fish.* **74**, 261-272.
Grubich, J. R. and Westneat, M. W. (2006). Four-bar linkage modelling in teleost pharyngeal jaws: computer simulations of bite kinetics. *J. Anat.* **209**, 79-92.
Hernandez, L. P. and Motta, P. J. (1997). Trophic consequences of differential performance in the sheepshead, *Archosargus probatocephalus* (Teleostei, Sparidae). *J. Zool. Lond.* **243**, 737-756.
Hilton, E. J. (2001). Tongue bite apparatus of osteoglossomorph fishes: variation of a character complex. *Copeia* **2001**, 372-381.
Hilton, E. J. (2003). Comparative osteology and phylognetic systematics of fossil and living bony-tongue fishes (Actinopterygii, Teleostei; Osteoglossomorpha). *Zool. J. Linn. Soc.* **137**, 1-100.
Ishiguro, N. B., Miya, M. and Nishida, M. (2003). Basal euteleostean relationships: a mitogenomic perspective on the phylogenetic reality of the "Protacanthopterygii". *Mol. Phylogenet. Evol.* **27**, 476-488.
Kershaw, D. R. (1976). A structural and functional interpretation of cranial anatomy in relation to the feeding of osteoglossoid fishes and a consideration of their phylogeny. *Trans. Zool. Soc. Lond.* **33**, 173-252.
Konow, N. and Sanford, C. P. J. (2008). Is a convergently derived muscle-activity pattern driving novel raking behaviors in teleost fishes? *J. Exp. Biol.* **211**, 989-999.
Konow, N., Camp, A. L. and Sanford, C. P. J. (2008). Congruence between muscle activity and kinematics in a convergently derived prey-processing behavior. *Integr. Comp. Biol.* **48**, 246-260.
Lauder, G. V. (1979). Feeding mechanisms in primitive teleosts and in the halecomorph fish *Amia calva. J. Zool. Soc. Lond.* **187**, 543-578.
Lauder, G. V. (1980). Evolution of the feeding mechanism in primitive actinopterygian fishes: a functional anatomical analysis of *Polypterus*, *Lepisosteus*, and *Amia. J. Morphol.* **163**, 283-317.
Lauder, G. V. (1981). Intraspecific functional repertoires in the feeding mechanism of the characoid fishes *Lebiasina, Hoplias* and *Chalceus. Copeia* **1981**, 154-168.
Lauder, G. V. (1982). Patterns of evolution in the feeding mechanism of actinopterygian fishes *Am. Zool.* **22**, 275-285.
Lauder, G. V. (1985). Aquatic feeding in lower vertebrates. In *Functional Vertebrate Morphology* (ed. M. Hildebrand, D. M. Bramble, K. F. Liem and D. B. Wake), pp. 210-229. Cambridge: Cambridge University Press.
Lauder, G. V. and Liem, K. F. (1980). The feeding mechanism and cephalic myology of *Salvelinus fontinalis*: form, function, and evolutionary significance. In *Charrs: Salomnids of the Genus* Salvelinus (ed. E. K. Balon), pp. 365-390. Netherlands: Junk Publishers.
Lauder, G. V. and Liem, K. F. (1983). The evolution and interrelationships of the Actinopterygian fishes. *Bull. Mus. Comp. Zool. Harvard.* **150**, 95-197.
Lauder, G. V. and Reilly, S. M. (1994). Amphibian feeding behavior: comparative biomechanics and evolution. In *Biomechanics of Feeding in Vertebrates: Advances in Comparative and Environmental Physiology* (ed. V. Bels, M. Chardon and P. Vandewalle), pp. 163-195. Berlin: Springer-Verlag.
Lavoué, S. and Sullivan, J. P. (2004). Simultaneous analysis of five molecular markers provides a well-supported phylogenetic hypothesis for the living bony-tongue fishes (Osteoglossomorpha: Teleostei). *Mol. Phylogenet. Evol.* **33**, 171-185.
Liem, K. F. (1984). The muscular basis of aquatic and aerial ventilation in the air-breathing teleost fish *Channa. J. Exp. Biol.* **113**, 1-18.
Liem, K. F. (1985). Ventilation. In *Functional Vertebrate Morphology* (ed. M. Hildebrand, D. M. Bramble, K. F. Liem and D. B. Wake), pp. 185-209. Cambridge: Cambridge University Press.
Liem, K. F. (1990). Aquatic versus terrestrial feeding modes: possible impacts on the trophic ecology of vertebrates. *Am. Zool.* **30**, 209-221.
Motta, P. J. (1984). The mechanics and functions of jaw protrusion in teleost fishes: a review. *Copeia.* **1984**, 1-18.
Muller, M. (1987). Optimization principles applied to the mechanism of neurocranium levation and mouth bottom depression in bony fishes (Halecostomii). *J. Theor. Biol.* **126**, 346-368.
Muller, M. (1989). A quantitative theory of expected volume changes of the mouth during feeding in teleost fishes. *J. Zool. Lond.* **217**, 639-662.
Muller, M. (1996). A novel classification of planar four-bar linkages and its application to the mechanical analysis of animal systems. *Proc. R. Soc. B.* **351**, 689-720.
Muller, M. and Osse, J. W. M. (1984). Hydrodynamics of suction feeding in fish. *Trans. Zool. Soc. Lond.* **37**, 51-135.
Nelson, G. J. (1968). Gill arches of teleostean fishes of the division Osteoglossomorpha. *Zool. J. Linn. Soc.* **47**, 261-277.
Norden, C. R. (1961). Comparative osteology of representative salmonid fishes with particular reference to the grayling (*Thymallus arcticus*) and its phylogeny. *J. Fish. Res. Board Can.* **18**, 679-791.
Rand, D. M. and Lauder, G. V. (1981). Prey capture in the chain pickerel, *Esox niger*: Correlations between feeding and locomotor behaviour. *Can. J. Zool.* **59**, 1072-1078.
Richard, B. A. and Wainwright, P. C. (1995). Scaling the feeding mechanism of largemouth bass (*Micropterus salmoides*): kinematics of prey capture *J. Exp. Biol.* **198**, 419-433.
Ridewood, W. G. (1904). On the cranial osteology of the clupeoid fishes. *Proc. Zool. Soc. Lond.* **2**, 448-493.
Ridewood, W.G. (1905). On the cranial osteology of the fishes of the families Osteoglossidœ, Pantodontidœ, and Phractolœmidœ. *Zool. J. Linn. Soc.* **29**, 252-282.
Robinson, M. P. and Motta, P. J. (2002). Patterns of growth and the effects of scale on the feeding kinematics of the nurse shark (*Ginglymostoma cirratum*). *J. Zool. Lond.* **256**, 449-462.

Roos, G., Leysen, H., Van Wassenbergh, S., Herrel, A., Jacobs, P., Dierick, M., Aerts, P. and Adriaens, D. (2008). Linking morphology and motion: a test of a four-bar mechanism in seahorses. *Physiol. Biochem. Zool.* (In press).
Rosen, D. E. (1974). Phylogeny and zoogeography of salmoniform fishes and relationships of *Lepidogalaxias salamandroides*. *Bull. AMNH* **153**, 267-325.
Ross, C. F., Eckhardt, A., Herrel, A., Hylander, W. L., Metzger, K. A., Schaerlaeken, V., Washington, R. L. and Williams, S. H. (2007). Modulation of intra-oral processing in mammals and lepidosaurs. *Integr. Comp. Biol.* **47**, 118-136.
Sanford, C. P. J. (2000). Salmonoid fish osteology and phylogeny (Teleostei: Salmonoidei). *Theses Zoologicae* 33. Liechtenstein, ARG Gantner Verlag KG.
Sanford, C. P. J. (2001a). The novel 'tongue-bite apparatus' in the knifefish family Notopteridae (Teleostei: Osteoglossomorpha): are kinematic patterns conserved within a clade? *Zool. J. Linn. Soc.* **132**, 259-275.
Sanford, C. P. J. (2001b). Kinematic analysis of a novel feeding mechanism in the brook trout *Salvelinus fontinalis* (Teleostei: Salmonidae): behavioral modulation of a functional novelty. *J. Exp. Biol.* **204**, 3905-3916.
Sanford, C. P. J. and Lauder, G. V. (1989). Functional morphology of the "Tongue-Bite" in the Osteoglossomorph fish *Notopterus*. *J. Morphol.* **202**, 379-408.
Sanford, C. P. J. and Lauder, G. V. (1990). Kinematics of the tongue-bite apparatus in osteoglossomorph fishes *J. Exp. Biol.* **154**, 137-162.
Sanford, C. P. J. and Wainwright, P. C. (2002). Use of sonomicrometry demonstrates the link between prey capture kinematics and suction pressure in largemouth bass. *J. Exp. Biol.* **205**, 3445-3457.
Sass, G. G. and Motta, P. J. (2002). The effects of satiation on strike mode and prey capture kinematics in the largemouth bass, *Micropterus salmoides*. *Environ. Biol. Fishes* **65**, 441-454.
Schwenk, K. and Wagner, G. P. (2000). Function and the evolution of phenotypic stability: connecting pattern to process. *Am. Zool.* **41**, 552-563.
Sibbing, F. A. (1982). Pharyngeal mastication and food transport in the carp (*Cyprinus carpio* L.): a cineradiographic and electromyographic study. *J. Morphol.* **172**, 223-258.
Stearley, R. F. and Smith, G. R. (1993). Phylogeny of the pacific trouts and salmons (*Oncorhynchus*) and genera of the family Salmonidae. *Trans. Am. Fish. Soc.* **122**, 1-33.
Stiassny, M. L. J., Parenti, L. and Johnson, G. D. (1996). *Interrelationships of Fishes*, 496 pp. New York: Academic Press.
Taverne, L. (1979). Ostéologie, Phylogene`se et Systématique des téléostéens fossiles et actuels du super ordre des Ostéoglossomorphes. Troisième partie: evolution des structures ostéologiques et conclusions générales relatives à la phylogenèse et à la systématique du super ordre. *Bull. Acad. R. Belg. Cl. Sci.* **43**, 1-168.
Thys, T. (1997). Spatial variation in epaxial muscle activity during prey strike in largemouth bass (*Micropterus salmoides*). *J. Exp. Biol.* **200**, 3021-3031.
Turingan, R. G. and Wainwright, P. C. (1993). Morphological and functional bases of durophagy in the queen triggerfish, *Balistes vetula* (Pisces, tetraodontiformes). *J. Morphol.* **215**, 101-118.
Turingan, R. G., Wainwright, P. C. and Hensley, D. A. (1995). Interpopulation variation in prey use and feeding biomechanics in Caribbean triggerfish. *Oecologia* **102**, 296-304.
Van Wassenbergh, S., Aerts, P. and Herrel, A. (2006). Scaling of suction feeding performance in the catfish *Clarias gariepinus*. *Physiol. Biochem. Zool.* **79**, 43-56.
Van Wassenbergh, S., Herrel, A., Adriaens, D. and Aerts, P. (2005). A test of mouth-opening and hyoid-depression mechanisms during prey capture in a catfish. *J. Exp. Biol.* **208**, 4627-4639.
Van Wassenbergh, S., Herrel, A., Adriaens, D. and Aerts, P. (2007). Interspecific variation in sternohyoideus muscle morphology in clariid catfishes: functional implications for suction feeding. *J. Morphol.* **268**, 232-242.
Wagner, G. P. and Schwenk, K. (2000). Evolutionarily stable configurations: functional integration and the evolution of phenotypic stability. In *Evolutionary Biology*, Vol. 31 (ed. M. K. Hecht, R. J. MacIntyre and M. T. Clegg). New York: Kluwer Academic Press.
Wainwright, P. C. (2005). Functional morphology of the pharyngeal jaw apparatus. In *Biomechanics of Fishes* (ed. R. Shadwick and G. V. Lauder), pp. 77-101. Chicago: Elsevier.
Wainwright, P. C. and Turingan, R. G. (1993). Coupled versus uncoupled functional systems: motor plasticity in the queen triggerfish *Balistes vetula*. *J. Exp. Biol.* **180**, 209-227.
Wainwright, P. C., Bellwood, D. R., Westneat, M. W., Grubichm, J. R. and Hoey, A. S. (2004). A functional morphospace for the skull of labrid fishes: patterns of diversity in a complex biomechanical system. *Biol. J. Linn. Soc. Lond.* **82**, 1-25.
Westneat, M. W. (1991). Linkage biomechanics and evolution of the unique feeding mechanism of *Epibulus Insidiator* (Labridae: Teleostei) *J. Exp. Biol.* **159**, 165-184.
Westneat, M. W. (1994). Transmission of force and velocity in the feeding mechanisms of labrid fishes. *Zoomorphology* **114**, 103-118.
Westneat, M. W. (1995). Feeding, function, and phylogeny: analysis of historical biomechanics in labrid fishes using comparative methods. *Syst. Biol.* **44**, 361-383.
Westneat, M. W. (2003). A biomechanical model for analysis of muscle force, power output and lower jaw motion in fishes. *J. Theor. Biol.* **223**, 269-281.
Westneat, M. W. (2004). Evolution of levers and linkages in the feeding mechanisms of fishes. *Integr. Comp. Biol.* **44**, 378-389.
Wilga, C. D. and Sanford, C. P. (2008). Suction generation in white spotted bamboo sharks *Chiloscyllium plagiosum*. *J. Exp. Biol.* **211**, 3128-3138.
Zar, J. H. (1999). *Biostatistical Analysis*, 4th edn, 663 pp. New Jersey: Prentice Hall.